

A Measurement of the Quadrupole Power Spectrum in the Clustering of the 2dF QSO Survey

Kazuhiro YAMAMOTO, Masashi NAKAMICHI, Akinari KAMINO
Graduate School of Science, Hiroshima University, Higashi-Hiroshima, 735-8526, Japan

Bruce A. BASSETT

*Institute of Cosmology and Gravitation, University of Portsmouth, England and
SAAO, Observatory, Cape Town, South Africa*

Hiroaki NISHIOKA

Institute of Astronomy and Astrophysics, Academia Sinica, Taipei 106, Taiwan, R.O.C.

(Received ; accepted)

Abstract

We report a measurement of the quadrupole power spectrum in the two degree field (2dF) QSO redshift (2QZ) survey. The analysis uses an algorithm parallel to that for the estimation of the standard monopole power spectrum without first requiring computation of the correlation function or the anisotropic power spectrum. The error on the quadrupole spectrum is rather large but the best fit value of the bias parameter from the quadrupole spectrum is consistent with that from previous investigations of the 2dF data.

Key words: methods: numerical – quasars: general – cosmological parameters – large-scale structure of Universe

1. Introduction

Since large cosmological surveys are carried out in redshift space, the peculiar velocity of sources distorts the apparent spatial distribution of cosmological objects. These redshift-space distortions are one of the important effects in large redshift surveys (e.g., Suto et al. 2000a, Magira, Jing, Suto 2000). Redshift distortions can be classified into the linear distortion arising in the linear theory of density perturbation and the *Finger of God* effect arising in the nonlinear regime. It has been also pointed out that the geometrical effect from the expansion of the universe causes another apparent distortion in the distribution of cosmological objects, which is referred to as the cosmological redshift-space distortion or the geometric distortion (Alcock, Paczynski 1979, Ballinger, Peacock, Heavens 1996, Matsubara, Suto 1996). Thus the detection of the redshift-space distortion provides us with unique information about the peculiar velocity and expansion history of the universe.

In the Kilo-Aperture Optical Spectrograph (KAOS/WFMOS, see <http://www.noao.edu/kaos/>), one of the future large survey projects, it will be possible to confront in great detail the theoretical redshift-space distortions including the geometric distortion with observation (e.g., Yamamoto, Nishioka, Bassett 2005). Such surveys will provide significant dark energy constraints (Matsubara, Szalay 2003, Seo, Eisenstein 2003, Linder 2003, Blake, Glazebrook 2003, Yamamoto 2003;2004, Amendola et al.2005) using the baryon acoustic signatures, which have recently been detected clearly in the SDSS and 2df data sets. (Eisenstein et al. 2005, Cole et al. 2005, Yahata et al. 2005).

In general it is known that the redshift-space power spectrum on a constant hypersurface of the redshift z can be expanded as (Taylor, Hamilton 1996)

$$P(\mathbf{k}, z) = P(k, \mu, z) = \sum_{l=0,2,4,\dots} P_l(k, z) \mathcal{L}_l(\mu)(2l+1), \quad (1)$$

where $\mathcal{L}_l(\mu)$ is the Legendre polynomials, $\mu(=\cos\theta)$ is the directional cosine between the line of sight direction and \mathbf{k} (See Figure 1).¹ The monopole $P_0(k, z)$ represents the angular averaged power spectrum, what we mean by the power spectrum usually, and the quadrupole $P_2(k, z)$ represents the leading anisotropies in the power spectrum due to the redshift-space distortions. The odd moments vanish by symmetry. The quadrupole spectrum provides us with new information over what is available in the monopole power spectrum. In practice, the quadrupole spectrum reflects the peculiar and random velocity of samples (Kaiser 1987, Cole, Fisher, Weinberg 1994, Hamilton 1996). It has been shown that the quadrupole spectrum will be especially useful in breaking the degeneracy between the bias and the dark energy parameters when measurements of the power spectrum are good enough in future surveys (Yamamoto et al. 2005). Thus accurate measurement of the quadrupole spectrum can be important in characterizing

¹ Note that our definition of the multipole spectrum P_l is different from the conventional definition by the factor $2l+1$.

the redshift-space distortions quantitatively.

Pioneering work on the measurement of the quadrupole power spectrum was carried out by Cole, Fisher and Weinberg (1994) and Hamilton (1996, 1997) using galaxy redshift survey catalogs. Cole et al. (1994) presented a systematic method to estimate the quadrupole power spectrum through the anisotropic power spectrum. Using the method, Hatton and Cole (1999) estimated the β -factor from the quadrupole power spectrum in the two degree field (2dF) galaxy survey. In the work by Hamilton (1996,1997) the quadrupole power spectrum was obtained by the transformation of the correlation function. In the present work, however, we consider a different method to estimate the higher multipole moments of the power spectrum. Our method is parallel to the one widely used to measure the monopole power spectrum (Feldman, Kaiser, Peacock 1994, Yamamoto 2003) and allows us to obtain the multipoles of the redshift-space power spectrum without evaluating the correlation function or the anisotropic power spectrum. The difference between our method and that developed by Cole et al.(1994) is discussed in the next section.

This paper is organized as follows: In section 2, we explain the algorithm for estimating the multipole moments of the power spectrum. In section 3, we apply the method to the 2dF QSO sample and obtain the quadrupole power spectrum. Using the result we briefly discuss the constraint on the bias parameter. The last section is devoted to summary and discussions. Throughout this paper we use units in which the speed of light is unity, $c = 1$.

2. Method

Here we explain the optimal weighting scheme for estimating the multipole moments of the anisotropic (i.e. redshift-space) power spectrum. Our method developed here is unique and different from those developed previously. Our method does not require computation of the correlation function; c.f. Hamilton (1996). A similar method was developed by Cole et al. (1994), which also does not require the computation of the correlation function. However it requires estimating the anisotropic power spectrum. The difference between our method and their method will be discussed in detail below, however, the essence is as follows.

In the Cole et al. method, it is necessary to divide the sample into subsamples and introduce one line of sight direction for each subsample in order to explicitly define μ . Thus in the Cole et al method, the line of sight directions for all objects are regarded as the same in each divided subsample. In our method, however, we need neither divide the sample nor explicitly define μ , instead, we introduce μ for each pair of objects of the sample (see Figure 1). Furthermore, the multipole moments can be computed fully in parallel with the conventional monopole estimation (i.e. the 'usual power spectrum').

Throughout this paper, we use \mathbf{s} to denote the three dimensional coordinates in redshift space. We also use $n_g(\mathbf{s})$ and $\bar{n}(\mathbf{s})$ to denote real catalog and the expected mean number density. A fluctuation field is then defined via

$$F(\mathbf{s}) = n_g(\mathbf{s}) - \alpha n_s(\mathbf{s}), \quad (2)$$

where $n_g(\mathbf{s}) = \sum_i \delta(\mathbf{s} - \mathbf{s}_i)$ with \mathbf{s}_i being the location of the i th object of real catalog; similarly $n_s(\mathbf{s}) = \sum_j \delta(\mathbf{s} - \mathbf{s}_j)$ is the density of a synthetic catalog. The synthetic catalog is a set of random points without correlation, which can be constructed through random process by mimicking the selection function of the real catalog. Here we assume that the synthetic catalog has a mean number density $1/\alpha$ times that of the real catalog. The synthetic catalog provides an estimate for the mean number density in the absence of clustering, then it is useful to provide an estimator for the fluctuation field $F(\mathbf{s})$. From the definition of the random field $n_s(\mathbf{s})$, we assume (Feldman et al. 1994),

$$\langle n_g(\mathbf{s}_1)n_g(\mathbf{s}_2) \rangle = \bar{n}(\mathbf{s}_1)\bar{n}(\mathbf{s}_2)(1 + \xi(\mathbf{s}_1, \mathbf{s}_2)) + \bar{n}(\mathbf{s}_1)\delta(\mathbf{s}_1 - \mathbf{s}_2), \quad (3)$$

$$\langle n_s(\mathbf{s}_1)n_s(\mathbf{s}_2) \rangle = \alpha^{-2}\bar{n}(\mathbf{s}_1)\bar{n}(\mathbf{s}_2) + \alpha^{-1}\bar{n}(\mathbf{s}_1)\delta(\mathbf{s}_1 - \mathbf{s}_2), \quad (4)$$

$$\langle n_g(\mathbf{s}_1)n_s(\mathbf{s}_2) \rangle = \alpha^{-1}\bar{n}(\mathbf{s}_1)\bar{n}(\mathbf{s}_2), \quad (5)$$

where $\xi(\mathbf{s}_1, \mathbf{s}_2)$ denotes the two-point correlation function. Using these relations, we have

$$\langle F(\mathbf{s}_1)F(\mathbf{s}_2) \rangle = \bar{n}(\mathbf{s}_1)\bar{n}(\mathbf{s}_2)\xi(\mathbf{s}_1, \mathbf{s}_2) + (1 + \alpha)\bar{n}(\mathbf{s}_1)\delta(\mathbf{s}_1 - \mathbf{s}_2). \quad (6)$$

The estimator for the multipole moments of the power spectrum may be defined as follows (see Yamamoto, Nishioka, Taruya 2000),

$$R_l(\mathbf{k}) = \frac{\int d\mathbf{s}_1 \int d\mathbf{s}_2 \psi(\mathbf{s}_1, \mathbf{k}) \psi(\mathbf{s}_2, \mathbf{k}) F(\mathbf{s}_1) F(\mathbf{s}_2) e^{i\mathbf{k} \cdot (\mathbf{s}_1 - \mathbf{s}_2)} \mathcal{L}_l(\hat{\mathbf{s}}_h \cdot \hat{\mathbf{k}})}{\int d\mathbf{s} \bar{n}^2(\mathbf{s}) \psi(\mathbf{s}, \mathbf{k})^2}, \quad (7)$$

where $\mathbf{s}_h = (\mathbf{s}_1 + \mathbf{s}_2)/2$ and the 'hat' means the unit vector, and $\psi(\mathbf{s}, \mathbf{k})$ is a weight factor. As mentioned before, $\mathcal{L}_l(\mu)$ is the Legendre polynomials. (See also Figure 1 for the definition of variables). We can choose the weight factor so as to minimize the variance of the spectrum in order to optimize the performance of the estimator according to the local density field (see below).

Here we adopt the approximate formula

$$\xi(\mathbf{s}_1, \mathbf{s}_2) = \int \frac{d\mathbf{k}}{(2\pi)^3} P(\mathbf{k}, |\mathbf{s}_h|) e^{-i\mathbf{k} \cdot (\mathbf{s}_1 - \mathbf{s}_2)}, \quad (8)$$

where $P(\mathbf{k}, |\mathbf{s}_h|)$ is the power spectrum defined on a constant-time hypersurface. This expression is not strictly correct when the redshift \mathbf{s}_1 and \mathbf{s}_2 are very different. Thus (8) is justified within the distant observer approximation, $|\mathbf{s}_1 - \mathbf{s}_2| \ll |\mathbf{s}_1|, |\mathbf{s}_2|$, i.e., in case of short separation between \mathbf{s}_1 and \mathbf{s}_2 .

Using the above relations and under the distant observer approximation, the ensemble average of $R_l(\mathbf{k})$ is

$$\langle R_l(\mathbf{k}) \rangle = \frac{\int ds \bar{n}(\mathbf{s})^2 \psi(\mathbf{s}, \mathbf{k})^2 P(\mathbf{k}, |\mathbf{s}|) \mathcal{L}_l(\hat{\mathbf{s}} \cdot \hat{\mathbf{k}})}{\int ds \bar{n}^2(\mathbf{s}) \psi(\mathbf{s}, \mathbf{k})^2} + S_l(\mathbf{k}), \quad (9)$$

where

$$S_l(\mathbf{k}) = \frac{(1 + \alpha) \int ds \bar{n}(\mathbf{s}) \psi(\mathbf{s}, \mathbf{k})^2 \mathcal{L}_l(\hat{\mathbf{s}} \cdot \hat{\mathbf{k}})}{\int ds \bar{n}^2(\mathbf{s}) \psi(\mathbf{s}, \mathbf{k})^2}. \quad (10)$$

The estimator of the anisotropic power spectrum is obtained by subtracting the shotnoise $S_l(\mathbf{k})$, yielding

$$\mathcal{P}_l(\mathbf{k}) = R_l(\mathbf{k}) - S_l(\mathbf{k}). \quad (11)$$

Next we focus on the covariance of $\mathcal{P}_l(\mathbf{k})$, which is given by

$$\begin{aligned} \langle \Delta \mathcal{P}_l(\mathbf{k}) \Delta \mathcal{P}_l(\mathbf{k}') \rangle &= \langle [\mathcal{P}_l(\mathbf{k}) - \langle \mathcal{P}_l(\mathbf{k}) \rangle] [\mathcal{P}_l(\mathbf{k}') - \langle \mathcal{P}_l(\mathbf{k}') \rangle] \rangle \\ &= \langle \mathcal{P}_l(\mathbf{k}) \mathcal{P}_l(\mathbf{k}') \rangle - \langle \mathcal{P}_l(\mathbf{k}) \rangle \langle \mathcal{P}_l(\mathbf{k}') \rangle \\ &= \langle R_l(\mathbf{k}) R_l(\mathbf{k}') \rangle - \langle R_l(\mathbf{k}) \rangle \langle R_l(\mathbf{k}') \rangle. \end{aligned} \quad (12)$$

Assuming Gaussian statistics some calculation gives:

$$\begin{aligned} \langle F(\mathbf{s}_1) F(\mathbf{s}_2) F(\mathbf{s}_3) F(\mathbf{s}_4) \rangle &= \langle F(\mathbf{s}_1) F(\mathbf{s}_2) \rangle \langle F(\mathbf{s}_3) F(\mathbf{s}_4) \rangle \\ &\quad + \langle F(\mathbf{s}_1) F(\mathbf{s}_3) \rangle \langle F(\mathbf{s}_2) F(\mathbf{s}_4) \rangle \\ &\quad + \langle F(\mathbf{s}_1) F(\mathbf{s}_4) \rangle \langle F(\mathbf{s}_3) F(\mathbf{s}_2) \rangle, \end{aligned} \quad (13)$$

we have

$$\begin{aligned} \langle \Delta \mathcal{P}_l(\mathbf{k}) \Delta \mathcal{P}_l(\mathbf{k}') \rangle &= \left[\int ds \bar{n}(\mathbf{s})^2 \psi(\mathbf{s}, \mathbf{k})^2 \right]^{-1} \left[\int ds' \bar{n}(\mathbf{s}')^2 \psi(\mathbf{s}', \mathbf{k}')^2 \right]^{-1} \\ &\quad \times 2 \prod_{i=1}^2 \left[\int ds_i \psi(\mathbf{s}_i, \mathbf{k}) \right] \prod_{j=3}^4 \left[\int ds_j \psi(\mathbf{s}_j, \mathbf{k}') \right] \langle F(\mathbf{s}_1) F(\mathbf{s}_3) \rangle \langle F(\mathbf{s}_2) F(\mathbf{s}_4) \rangle \\ &\quad \times e^{i\mathbf{k} \cdot (\mathbf{s}_1 - \mathbf{s}_2)} e^{-i\mathbf{k}' \cdot (\mathbf{s}_3 - \mathbf{s}_4)} \mathcal{L}_l(\hat{\mathbf{s}}_h \cdot \hat{\mathbf{k}}) \mathcal{L}_l(\hat{\mathbf{s}}'_h \cdot \hat{\mathbf{k}}'), \end{aligned} \quad (14)$$

where $\mathbf{s}_h = (\mathbf{s}_1 + \mathbf{s}_2)/2$ and $\mathbf{s}'_h = (\mathbf{s}_3 + \mathbf{s}_4)/2$. Repeatedly using the distant observer approximation,

$$\begin{aligned} &\int d\mathbf{s}_1 \int d\mathbf{s}_3 \psi(\mathbf{s}_1, \mathbf{k}) \psi(\mathbf{s}_3, \mathbf{k}') \langle F(\mathbf{s}_1) F(\mathbf{s}_3) \rangle e^{i\mathbf{k} \cdot \mathbf{s}_1 - i\mathbf{k}' \cdot \mathbf{s}_3} \\ &\quad \simeq \int ds \bar{n}(\mathbf{s})^2 \psi(\mathbf{s}, \mathbf{k}) \psi(\mathbf{s}, \mathbf{k}') e^{i\mathbf{s} \cdot (\mathbf{k} - \mathbf{k}')} \left[P\left(\frac{\mathbf{k} + \mathbf{k}'}{2}, |\mathbf{s}|\right) + \frac{\alpha + 1}{\bar{n}(\mathbf{s})} \right], \end{aligned} \quad (15)$$

we finally have

$$\langle \Delta \mathcal{P}_l(\mathbf{k}) \Delta \mathcal{P}_l(\mathbf{k}') \rangle \simeq \overline{\Delta P_l^2}(\mathbf{k}) \delta^{(3)}(\mathbf{k} - \mathbf{k}'), \quad (16)$$

where

$$\overline{\Delta P_l^2}(\mathbf{k}) = 2(2\pi)^3 \frac{\int ds \bar{n}(\mathbf{s})^4 \psi(\mathbf{s}, \mathbf{k})^4 [P(\mathbf{k}, |\mathbf{s}|) + (1 + \alpha)/\bar{n}(\mathbf{s})]^2 [\mathcal{L}_l(\hat{\mathbf{k}} \cdot \hat{\mathbf{s}})]^2}{[\int ds' \bar{n}(\mathbf{s}')^2 \psi(\mathbf{s}', \mathbf{k})^2]^2}. \quad (17)$$

We define the estimator of the multipole moments of the anisotropic power spectrum by

$$\mathcal{P}_l(k) = \frac{1}{\Delta V_k} \int_{\Delta V_k} d\mathbf{k} \mathcal{P}_l(\mathbf{k}), \quad (18)$$

where ΔV_k denotes the volume of the shell in the Fourier space. The ensemble average of $\mathcal{P}_l(k)$ is given by

$$\langle \mathcal{P}_l(k) \rangle = \frac{1}{\Delta V_k} \int_{\Delta V_k} d\mathbf{k} \frac{\int ds \bar{n}(\mathbf{s})^2 \psi(\mathbf{s}, \mathbf{k})^2 P(\mathbf{k}, |\mathbf{s}|) \mathcal{L}_l(\hat{\mathbf{k}} \cdot \hat{\mathbf{s}})}{\int ds' \bar{n}^2(\mathbf{s}') \psi(\mathbf{s}', \mathbf{k})^2}. \quad (19)$$

Note that $\mathcal{P}_l(k)$ corresponds to the multipole coefficient $P_l(k, z)$ in equation (1). $\mathcal{P}_l(k)$ is generalized so as to incorporate the redshift evolution. In the limit that the sources are confined to a very narrow range of redshifts z , $\langle \mathcal{P}_l(k) \rangle$ reduces to $P_l(k, z)$.

The variance of $\mathcal{P}_l(k)$ is obtained by evaluating

$$\begin{aligned} \langle \Delta \mathcal{P}_l(k)^2 \rangle &\equiv \langle [\mathcal{P}_l(k) - \langle \mathcal{P}_l(k) \rangle]^2 \rangle \\ &= \frac{1}{\Delta V_k^2} \int_{\Delta V_k} d\mathbf{k} \int_{\Delta V_k} d\mathbf{k}' \langle \Delta \mathcal{P}_l(\mathbf{k}) \Delta \mathcal{P}_l(\mathbf{k}') \rangle, \end{aligned} \quad (20)$$

which reduces to

$$\langle \Delta \mathcal{P}_l(k)^2 \rangle = 2 \frac{(2\pi)^3}{\Delta V_k} \mathcal{Q}_l^2(\mathbf{s}, k), \quad (21)$$

where we have defined

$$\mathcal{Q}_l^2(\mathbf{s}, k) = \frac{1}{\Delta V_k} \int_{\Delta V_k} d\mathbf{k} \frac{\int ds \bar{n}(\mathbf{s})^4 \psi(\mathbf{s}, \mathbf{k})^4 [P(\mathbf{k}, |\mathbf{s}|) + 1/\bar{n}(\mathbf{s})]^2 [\mathcal{L}_l(\hat{\mathbf{k}} \cdot \hat{\mathbf{s}})]^2}{[\int ds' \bar{n}(\mathbf{s}')^2 \psi(\mathbf{s}', \mathbf{k})^2]^2}. \quad (22)$$

Here we have assumed $\alpha \ll 1$.

Now we find that the following weight factor gives the stationary solution ²

$$\psi(\mathbf{s}, \mathbf{k}) = \frac{1}{1 + \bar{n}(\mathbf{s})P(\mathbf{k}, |\mathbf{s}|)} \quad (23)$$

for the variation

$$\frac{\delta \langle \Delta \mathcal{P}_l(k)^2 \rangle}{\delta \psi(\mathbf{s}, \mathbf{k})} = 0. \quad (24)$$

In this case find the minimum error

$$\langle \Delta \mathcal{P}_l(k)^2 \rangle = 2 \frac{(2\pi)^3}{\Delta V_k} \frac{1}{2} \int_{-1}^1 d\mu \frac{[\mathcal{L}_l(\mu)]^2}{\int ds' \bar{n}(\mathbf{s}')^2 [1 + \bar{n}(\mathbf{s}')P(k, \mu, |\mathbf{s}'|)]^{-2}}, \quad (25)$$

where we used the notation $\mu = \hat{\mathbf{k}} \cdot \hat{\mathbf{s}}$, $\psi(\mathbf{s}, \mathbf{k}) = \psi(\mathbf{s}, k, \mu)$ and $P(\mathbf{k}, |\mathbf{s}|) = P(k, \mu, |\mathbf{s}|)$. In the case $\bar{n}P(\mathbf{k}, |\mathbf{s}|) \ll 1$, we may set $\psi(\mathbf{s}, \mathbf{k}) = 1$ and we have

$$(2l+1) \langle \Delta \mathcal{P}_l(k)^2 \rangle = \langle \Delta \mathcal{P}_0(k)^2 \rangle = 2 \frac{(2\pi)^3}{\Delta V_k} \frac{1}{\int ds' \bar{n}(\mathbf{s}')^2}, \quad (26)$$

where we assumed the Legendre polynomials are normalized by

$$\int_{-1}^1 d\mu \mathcal{L}_l(\mu) \mathcal{L}_{l'}(\mu) = \frac{2}{2l+1} \delta_{ll'}. \quad (27)$$

Thus the error of the l -th moment is smaller than in the monopole spectrum by $\sqrt{2l+1}$.

Here we summarize the difference between our method and that developed by Cole et al. (1994). Using our notation, essentially, they first estimate

$$\frac{\int ds_1 \int ds_2 \psi(\mathbf{s}_1, \mathbf{k}) \psi(\mathbf{s}_2, \mathbf{k}) F(\mathbf{s}_1) F(\mathbf{s}_2) e^{i\mathbf{k} \cdot (\mathbf{s}_1 - \mathbf{s}_2)}}{\int ds \bar{n}^2(\mathbf{s}) \psi(\mathbf{s}, \mathbf{k})^2} \equiv R(\mathbf{k}), \quad (28)$$

which is same as the right hand side of equation (7) but without $\mathcal{L}_l(\hat{\mathbf{s}}_h \cdot \hat{\mathbf{k}})$. After averaging $R(\mathbf{k})$ over the angle φ (Figure 1), and subtracting the shotnoise contribution, the anisotropic power spectrum $P(k, \mu)$ can be obtained. Then the quadrupole component can be obtained from $P(k, \mu)$ using $\mathcal{L}_l(\mu)$. In order to define the direction of the line of sight, in their method, a Gaussian window function is introduced, and the above procedure is repeated for the sample with different windows and the result is averaged. Essentially, in their method, the sample is divided into subsamples in order to clearly introduce the quantity μ associated with a line of sight direction. Thus the method by Cole et al.(1994) first requires computation of the anisotropic power spectrum, whilst our method does not. The estimation of the multipole spectrum can be performed completely parallel with that for the estimation of the monopole spectrum. However, in principle, both the methods are equivalent in the limit of the distant observer approximation (excepting the weight factor).

² Compare with the result in (Yamamoto 2003), in which the weighting factor was determined under the constraint that it has no angular dependence $\psi(\mathbf{s}, \mathbf{k}) = \psi(\mathbf{s}, k)$.

Next let us consider the estimator for the discrete density field of the object catalog. In this case we replace $\mathcal{L}_l(\hat{\mathbf{s}}_n \cdot \hat{\mathbf{k}})$ in equation (7) with $\mathcal{L}_l(\hat{\mathbf{s}}_1 \cdot \hat{\mathbf{k}})$, which is valid as long as the distant observer approximation is applicable, and then we may write

$$R_l(\mathbf{k}) = A^{-1} \left(\sum_{i_1}^N \psi(\mathbf{s}_{i_1}, \mathbf{k}) e^{i\mathbf{k} \cdot \mathbf{s}_{i_1}} \mathcal{L}_l(\hat{\mathbf{s}}_{i_1} \cdot \mathbf{k}) - \alpha \sum_{j_1}^{N_s} \psi(\mathbf{s}_{j_1}, \mathbf{k}) e^{i\mathbf{k} \cdot \mathbf{s}_{j_1}} \mathcal{L}_l(\hat{\mathbf{s}}_{j_1} \cdot \mathbf{k}) \right) \\ \times \left(\sum_{i_2}^N \psi(\mathbf{s}_{i_2}, \mathbf{k}) e^{i\mathbf{k} \cdot \mathbf{s}_{i_2}} - \alpha \sum_{j_2}^{N_s} \psi(\mathbf{s}_{j_2}, \mathbf{k}) e^{i\mathbf{k} \cdot \mathbf{s}_{j_2}} \right), \quad (29)$$

where N (N_s) is the number of objects of the real (synthetic) catalog, respectively, and we have defined $A = \int d\mathbf{s} \bar{n}(\mathbf{s})^2 \psi(\mathbf{s}, \mathbf{k})^2$. In a similar way, the shotnoise term may be written as

$$S_l(\mathbf{k}) = A^{-1} (1 + \alpha) \sum_i^N \psi(\mathbf{s}_i, \mathbf{k})^2 \mathcal{L}_l(\hat{\mathbf{s}}_i \cdot \mathbf{k}), \quad (30)$$

using the real catalog, or

$$S_l(\mathbf{k}) = A^{-1} (1 + \alpha) \alpha \sum_j^{N_s} \psi(\mathbf{s}_j, \mathbf{k})^2 \mathcal{L}_l(\hat{\mathbf{s}}_j \cdot \mathbf{k}), \quad (31)$$

using the synthetic catalog. The other possible expression is

$$S_l(\mathbf{k}) = A^{-1} \left(\sum_i^N \psi(\mathbf{s}_i, \mathbf{k})^2 \mathcal{L}_l(\hat{\mathbf{s}}_i \cdot \mathbf{k}) + \alpha^2 \sum_j^{N_s} \psi(\mathbf{s}_j, \mathbf{k})^2 \mathcal{L}_l(\hat{\mathbf{s}}_j \cdot \mathbf{k}) \right), \quad (32)$$

using both the real and synthetic catalogs, as used in Cole et al. (2005). The choice of the shotnoise estimation does not alter our results in the present paper.

3. Application to the 2QZ survey

In this section, we apply the method to the 2dF QSO sample. In general, the constraint on the cosmological parameters from the QSO sample is not very tight, however, it is useful to obtain unique information about the high redshift universe. The clustering of the sample has been investigated by the 2QZ group extensively (e.g., Outram et al. 2003, Croom et al. 2005 and references therein). The result from the clustering analysis is quite consistent with the prediction of the concordance Λ cold dark matter (CDM) model built up from consideration of other cosmological data (e.g., Spergel et al. 2003, Cole et al. 2005, Tegmark et al. 2004, Riess et al. 1998, Perlmutter et al. 1999). The redshift-space distortion in the clustering of the 2QZ sample has been investigated by Outram et al. (2004). In their work, the anisotropic power spectrum $P(k_{\parallel}, k_{\perp})$ is measured, and the value of $\beta (= \Omega_m^{0.6}/b)$ is determined, where k_{\parallel} and k_{\perp} are the wave numbers parallel and perpendicular to the line of sight direction, respectively. In contrast to their approach we focus on the quadrupole spectrum in the clustering of the 2QZ sample.

The present work is an extension of previous work investigating the monopole power spectrum with the 2QZ sample (Yamamoto 2004). Here we briefly review the survey details for self-containment. The 2QZ survey covers two areas of $5 \times 75 \text{ deg}^2$, one in the south Galactic cap (SGC) and the other in the north Galactic cap (NGC) in the redshift range of less than 3. The survey area is defined by the equatorial coordinates from $\alpha = 21^{\text{h}}40$ to $\alpha = 3^{\text{h}}15$ and $-32.5^\circ \leq \delta \leq -27.5^\circ$ in the SGC, and $9^{\text{h}}50 \leq \alpha \leq 14^{\text{h}}50$ and $-2.5^\circ \leq \delta \leq 2.5^\circ$ in the NGC, respectively.

We use the final catalog reported by the 2QZ survey group, which is available through the home page <http://www.2dfquasar.org/>. Details of the QSO selection of the catalog is also described in the reference Croom et al. 2004, in which the photometric and spectroscopic incompleteness is discussed, as well as the angular selection function. The coverage incompleteness is given by the hole information which is publicly available through the home page. We generate the random sample through a random process mapping angular position of a QSO to different position with fixing the redshift with an equal probability on each survey area. Then we use 10713 and 8442 QSOs in the SGC and the NGC, respectively, in the range of redshift $0.2 \leq z \leq 2.2$ incorporating the hole information. Outram et al. (2004) used the QSOs in the range of redshift $0.3 \leq z \leq 2.2$, which is slightly different from our choice. This difference does not alter our result because the number of the QSOs in the range $0.2 \leq z \leq 0.3$ is less than one percent of the total number of the QSOs used here.

Next we explain our theoretical modeling of the power spectrum. In a redshift survey, the redshift z is the indicator of the distance. Therefore we need to assume a distance-redshift relation $s = |\mathbf{s}| = s(z)$ to plot a map of objects. The

power spectrum depends on this choice of the radial coordinate of the map $s = s(z)$ due to the geometric distortion. For the Λ CDM model the comoving distance is given by

$$r(z, \Omega_m) = \int_0^z \frac{dz'}{H_0 \sqrt{\Omega_m(1+z')^3 + 1 - \Omega_m}}, \quad (33)$$

where $H_0 = 100 \text{ km/s/Mpc}$ is the Hubble parameter. For our fiducial model we adopt the flat Λ CDM model with $\Omega_m = 0.3$. Thus our fiducial model is $s(z) = r(z, 0.3)$.

Our theoretical model properly incorporates the light-cone effect (redshift-evolution effect of the clustering), the geometric distortion, the linear distortion, the Finger of God effects, including the nonlinear evolution of the density perturbations. We model the QSO power spectrum as (e.g., Suto et al. 2000b, Yamamoto 2002; 2003)

$$P(\mathbf{k}, s(z)) = P(k, \mu, s(z)) = \frac{s(z)^2}{r(z)^2} \frac{ds(z)}{dr(z)} P_{QSO} \left(q_{\parallel} \rightarrow k \mu \frac{ds(z)}{dr(z)}, q_{\perp} \rightarrow k \sqrt{1 - \mu^2} \frac{s(z)}{r(z)} \right) \quad (34)$$

with

$$P_{QSO}(q_{\parallel}, q_{\perp}) = b(z)^2 \left(1 + \frac{d \ln D_1(z) / d \ln a(z)}{b(z)} \frac{q_{\parallel}^2}{q^2} \right)^2 P_{\text{mass}}^{\text{Nonlinear}}(q, z) D[q_{\parallel} \sigma_P(z)] \mathcal{D}(\delta z) \quad (35)$$

for the nonlinear modeling, and

$$P_{QSO}(q_{\parallel}, q_{\perp}) = b(z)^2 \left(1 + \frac{d \ln D_1(z) / d \ln a(z)}{b(z)} \frac{q_{\parallel}^2}{q^2} \right)^2 P_{\text{mass}}^{\text{Linear}}(q, z) \mathcal{D}(\delta z) \quad (36)$$

for the linear modeling, where $q^2 = q_{\parallel}^2 + q_{\perp}^2$, $D_1(z)$ is the linear growth factor normalized to $D_1(z=0) = 1$, $P_{\text{mass}}^{\text{Linear}}(q, z)$ ($P_{\text{mass}}^{\text{Nonlinear}}(q, z)$) is the linear (nonlinear) mass power spectrum, $D[q_{\parallel} \sigma_P(z)]$ is the damping factor due to the Finger of God effect, and $\mathcal{D}(\delta z)$ represents the damping factor due to the error in redshift measurement (see equation (37)). We model the exponential distribution function for the pairwise peculiar velocity, using an approximate formula for the mean square velocity dispersion at the large separation determined through the cosmic energy equation (Mo et al. 1997, Magira et al. 2000, Suto et al. 2000a). In particular for the QSO sample, the error in measuring the redshift is not negligible, which causes an apparent velocity dispersion and additional redshift-space distortion. We incorporate this effect in modeling the power spectrum by multiplying the spectrum with the damping factor

$$\mathcal{D}(\delta z) = \exp \left[-k_{\parallel}^2 \left\langle \left(\frac{ds}{dz} \right)^2 < \delta z^2 > \right. \right], \quad (37)$$

where k_{\parallel} is the comoving wave number parallel to the line of sight direction, δz is the variance in the redshift measurement error for which we adopt $\delta z = 0.0014(1+z)$ (Croom et al. 2005).

In the modeling of the bias, we consider the scale independent bias model of Fry (1996)

$$b(z) = 1 + \frac{b_0 - 1}{D_1(z)}, \quad (38)$$

where b_0 is the constant bias parameter.

Figure 2 plots our theoretical curves for $\mathcal{P}_0(k)$ (left panel) and $\mathcal{P}_2(k)/\mathcal{P}_0(k)$ (right panel), to show which effect is important in the power spectrum. The upper (lower) panel assumes $b_0 = 1$ ($b_0 = 2$) in the bias model (38). Here we adopt the other cosmological parameters $\Omega_m = 0.28$, $\Omega_b = 0.045$, $h = 0.7$, $\sigma_8 = 0.9$ and $n = 1$ motivated the WMAP result (Spergel et al. 2003). In this figure the dashed curve is the linear modeling (36), while the solid curve is the nonlinear modeling (35). Concerning the monopole spectrum \mathcal{P}_0 , the linear model is very similar to the nonlinear model. This occurs by a cancellation effect of the two nonlinear effects; One is the increase of the amplitude of the real-space power spectrum at large k . The other is the decrease of the amplitude due to the damping factor of the Finger of God effect $D[q_{\parallel} \sigma_P(z)]$ and the error in redshift measurement $\mathcal{D}(\delta z)$. Concerning the quadrupole divided by the monopole, $\mathcal{P}_2/\mathcal{P}_0$, the behavior at small k comes from the linear distortion effect, while the behavior at large k comes from the damping factor $\mathcal{D}(\delta z)$ (dashed curve). In the absence of $\mathcal{D}(\delta z)$, $\mathcal{P}_2/\mathcal{P}_0$ is constant for k in the linear modeling. In the nonlinear model of $\mathcal{P}_2/\mathcal{P}_0$ (solid curve), the further decrease appears due to the Finger of God effect, though the effect is not very significant. This suggests that the error in redshift measurement is the significant effect in the present sample for \mathcal{P}_2 . The effect of the geometric distortion is negligibly small in our model because the fiducial model to plot map and the theoretical model is very close. Namely, $s(z)$ and $r(z)$ are not very different.

Then we followed the prescription explained in the previous section for the multipole moments of the power spectrum. We generated the random catalog with the parameter choice $\alpha = 1/15$. Figure 3 plots the monopole power spectrum (open squares on the upper panels) and the quadrupole spectrum divided by the monopole spectrum (open squares on the lower panels). The left and right panels show the results with the SGC and NGC samples, respectively. The error bars are estimated from the expression (26). The solid curve in Figure 3 is the theoretical curve of the Λ CDM model

with the cosmological parameters same as those of Figure 2, and $b_0 = 1.5$ the best fit value of the bias parameter. For small wave numbers less than $k < 0.03h\text{Mpc}^{-1}$, the measured quadrupole has negative sign.

Here let us briefly compare our approach with that of Outram et al. (2004). As mentioned before, they measured the anisotropic power spectrum $P(k_{\parallel}, k_{\perp})$, while we have measured the quadrupole moment $\mathcal{P}_2(k)$. In their analysis, in order to estimate $P(k_{\parallel}, k_{\perp})$, each $5 \times 75 \text{ deg}^2$ strip was divided into 8 regions. And for each of these small region, k_{\parallel} and k_{\perp} were defined by applying the distant observer approximation. Thus $P(k_{\parallel}, k_{\perp})$ were estimated separately in 16 individual $5 \times 10 \text{ deg}^2$ regions. We have also estimated the quadrupole spectrum in these divided samples, but the method clearly failed to detect the quadrupole spectrum. As the area of the individual region becomes small, the estimated values of the quadrupole spectrum become negative. This suggests that the quadrupole spectrum with our method is sensitive to the shape and the boundary of the survey area of the sample.

Earlier work investigated the constraints from 2QZ on the cosmological parameters Ω_m , Ω_b and the equation of state of the dark energy w , by fitting to the monopole power spectrum (Yamamoto 2002, 2004). In the present work, by adopting the above theoretical model, we compare the measured quadrupole spectrum with the theoretical prediction. Using the bias model (38), for this comparison we define

$$\chi^2 = \sum_i \frac{[\mathcal{P}_l(k_i)^{\text{th}} - \mathcal{P}_l(k_i)^{\text{ob}}]^2}{\Delta \mathcal{P}_l(k_i)^2}, \quad (39)$$

where $\mathcal{P}_l(k_i)^{\text{ob}}$ is the value of the observed power spectrum at k_i , $\Delta \mathcal{P}_l(k_i)$ is the variance of errors in Figure 3, and $\mathcal{P}_l(k_i)^{\text{th}}$ is the theoretical spectrum predictions. Figure 4 shows χ^2 as a function of the bias parameter b_0 . The left and right panels show the results for the SGC and NGC samples, respectively. Here we fixed the other cosmological parameters to be the same as those in Figure 2. The degree of freedom is 12. In each panel, the dashed curve is the result from \mathcal{P}_0 , the best fit value of b_0 is 1.4 (1.5) for the SGC (NGC) sample. On the other hand, the solid curve is the result from the quadrupole, \mathcal{P}_2 . Because the error of \mathcal{P}_2 is larger than from \mathcal{P}_0 , the constraint on b_0 from \mathcal{P}_2 is weak. However, we see the minimum of χ^2 of the solid curve is located around the minimum of the dashed curve in the left panel. These are consistent with the best fit value of $b_0 = 1.64$ found by the 2QZ group though the assumed cosmological model is slightly different from ours (Croom et al. 2005).

For the right panel (NGC), the agreement is not good compared with the SGC sample, but we see roughly the same behavior, although there are some troubling discrepancies that deserve further study. We may conclude that the quadrupole signal is detected in our analysis, though the error is rather large. As the reason of the poor detection, we infer a contamination of the systematic error due to the survey geometry, i.e., the shape and the boundary effect of the inhomogeneous survey region.

Here we discuss the validity of bias model. As is mentioned by Croom et al.(2001;2005), the redshift-evolution of bias (38) does not fit observational data very much. They have given the best fit formula (Croom et al.2005).

$$b(z) = 0.53 + 0.289(1+z)^2. \quad (40)$$

The dashed curve in Figure 3 plots the theoretical one using this fit formula of the bias evolution. We see the good agreement between the dashed curve and the solid curve. Note that the solid curve is the theoretical curve using the bias model (38). This agreement comes from the fact that our theoretical spectrum depends only on a mean value of the bias.

Finally in this section, we briefly mention the validity of the distant observer approximation. Cole et al.(1994) discussed various effects which affect the proper β -factor estimation from the redshift-space distortion. A possible relevant effect here is the large opening angle on the survey. Cole et al.(1994) found that a correction might be needed to be applied for angles greater than 30 degree. However, the range of the redshift of the 2QZ sample is large. At a mean redshift $z = 1.2$, the wave number $k = 2\pi/\lambda$ is less than $0.005 h\text{Mpc}^{-1}$ for $\lambda = s(z)\sin(\theta)$ with $\theta = 30$ degree. Thus the distant observer approximation is good in our situation. On the other hand for $\theta = 5$ degree, $k \simeq 0.03 h\text{Mpc}^{-1}$, therefore deviations in the observed quadrupole spectrum away from the theoretical prediction may appear around these wavenumbers.

4. Conclusions

In summary we have investigated the quadrupole of the redshift-space power spectrum, $P_2(k)$, of the 2dF QSO survey. First, we have developed an algorithm which estimates the quadrupole and monopole spectra in a unified manner. The error in a measurement of the quadrupole spectrum is given analytically. We have detected the signal of the redshift distortions in the quadrupole spectrum, though the errors are still substantial.

When we used the sample divided into several subsamples, the agreement of the estimated spectrum with the theoretical model became worse. However, the resulting power spectrum is consistent with the theoretical prediction and with previous analysis of the 2QZ survey. Concerning the bias, however, as discussed by Croom et al. (2001;2005), the Fry bias model is not the best fitting model for the evolution of the QSO bias. To check a more realistic model of

the bias, we used the formula (40) in the theoretical modeling, which best fits the data from Croom et al.(2005). We found that this theoretical curve is almost the same as that of the Fry's bias model. This is because our theoretical spectrum depends only on the mean value of the bias.

Constraining the nature of dark energy is one of the ultimate purposes of such a clustering analysis. However, as demonstrated in (Yamamoto 2004), the 2dF QSO sample cannot provide a stringent constraint on the equation of state of the dark energy. The reason for this is the large shotnoise in the QSO distribution since the mean number density is too small. The application of the algorithm tested here to other, larger, galaxy samples such as SDSS will be very interesting (see e.g., Eisenstein et al. 2005, Cole et al. 2005, Yahata et al. 2005) and is left to future work.

Acknowledgments We thank the anonymous referee for useful comments, which helped improve the manuscript. This work is supported by Grant-in-Aid for Scientific Research of Japanese Ministry of Education, Culture, Sports, Science, and Technology 15740155.

References

- Alcock, C., Paczynski, B. 1979, *Nature*, 281, 358
 Amendola, L., Quercellini, C., Giallongo, E. 2005, *MNRAS*, 357, 429
 Ballinger, W. E., Peacock, J. A., Heavens, A. F., *MNRAS* 1996, 282, 877
 Blake, C., Glazebrook, K. 2003, *ApJ* 594, 665
 Cole, S., Fisher, K. B., Weinberg, D. H. 1994, *MNRAS*, 267, 799
 Cole, S., et al.2005, *MNRAS* in press; (astro-ph/0501174)
 Croom, S. M., Shanks, T., Boyle, B. J., Smith, R. J., Miller, L., Loaring, N. S., Hoyle, F. 2001, *MNRAS*, 325, 483
 Croom, S. M., Smith, R. J., Boyle, B. J., Shanks, T., Miller, L., Outram, P. J., Loaring, N. S. 2004, *MNRAS*, 349, 1397
 Croom, S. M., Boyle, B. J., Shanks, T., Smith, R. J., Miller, L., Outram, P. J., Loaring, N. S., Hoyle, F., da Angela, J. 2005, *MNRAS* in press (astro-ph/0490314)
 Eisenstein, D. J., et al. 2005; astro-ph/0501171
 Feldman, H. A., Kaiser, N., Peacock, J. A. 1994, *ApJ*, 426, 23
 Fry, N. J. 1996,*ApJ*, 578, 90
 Linder, E. V. 2003, *Phys. Rev. D*68 083504
 Hamilton, A. J. S. 1997, in the *Proceedings of Ringberg Workshop on Large-Scale Structure*, ed. D. Hamilton; (astro-ph/9708012)
 Hamilton, A. J. S. 1996, in the *Clustering in the Universe*, Proceedings XVth Rencontres de Moriond, ed. S. Maurogordato, et al.; (astro-ph/9507022)
 Hatton, S., Cole, S, 1999, *MNRAS*, 310, 1146
 Kaiser, N., 1987, *MNRAS*, 227, 1
 Magira, H., Jing, Y. P., Suto, Y. 2000, *ApJ*, 528, 30
 Matsubara, T., Suto, Y. 1996, *ApJ*, 470, L1
 Matsubara, T., Szalay, A. S. 2003, *Phys. Rev. Lett.* 90, 1302
 Mo, J., Jing, Y. P., Boerner, G. 1997, *MNRAS*, 286, 979
 Outram, P.J., Hoyle, F., Shanks, T., Croom, S. M., Boyle, B. J., Miller, L., Smith, R. J., & Myers, A. D. 2003 *MNRAS*, 342, 483
 Outram, P.J., Shanks, T., Boyle, B. J., Croom, S. M., Hoyle, F., LOaring N. S., Miller, L., Smith, R. J. 2004, *MNRAS*, 348, 745
 Perlmutter, S. et al.1999, *ApJ*, 517, 565
 Riess, A. G. et al.1998, *Astron. J.* 116, 1009
 Seo, H-J, Eisenstein D. J., 2003 *ApJ*, 598 720.
 Spergel, D. N., et al.2003, *ApJS*, 148, 175
 Suto, Y., Magira, H., Jing, Y. P., Matsubara, T., Yamamoto, K. 2000a, *Prog. Theor. Phys. Suppl.* 133, 183
 Suto Y., Magira H., Yamamoto, K. 2000b, *Publ. Astron. Soc. Japan*, 52, 249,
 Taylor, A. N., Hamilton, A. J. S. 1996, *MNRAS*, 282, 767
 Tegmark, M. et al.2004, *Phys. Rev. D*69 103501
 Yahata, K., et al. 2005; *Publ.Astron.Soc.Jap.* 57, 529
 Yamamoto, K., Nishioka, H., Taruya, A. 2000, unpublished; (astro-ph/0012433)
 Yamamoto, K. 2002, *MNRAS*, 334, 958
 Yamamoto, K. 2003, *ApJ*, 595, 577
 Yamamoto, K. 2004, *ApJ*, 605, 620
 Yamamoto, K., Nishioka, H., Bassett, B. A. 2005, *Phys. Rev. Lett* 94, 051301

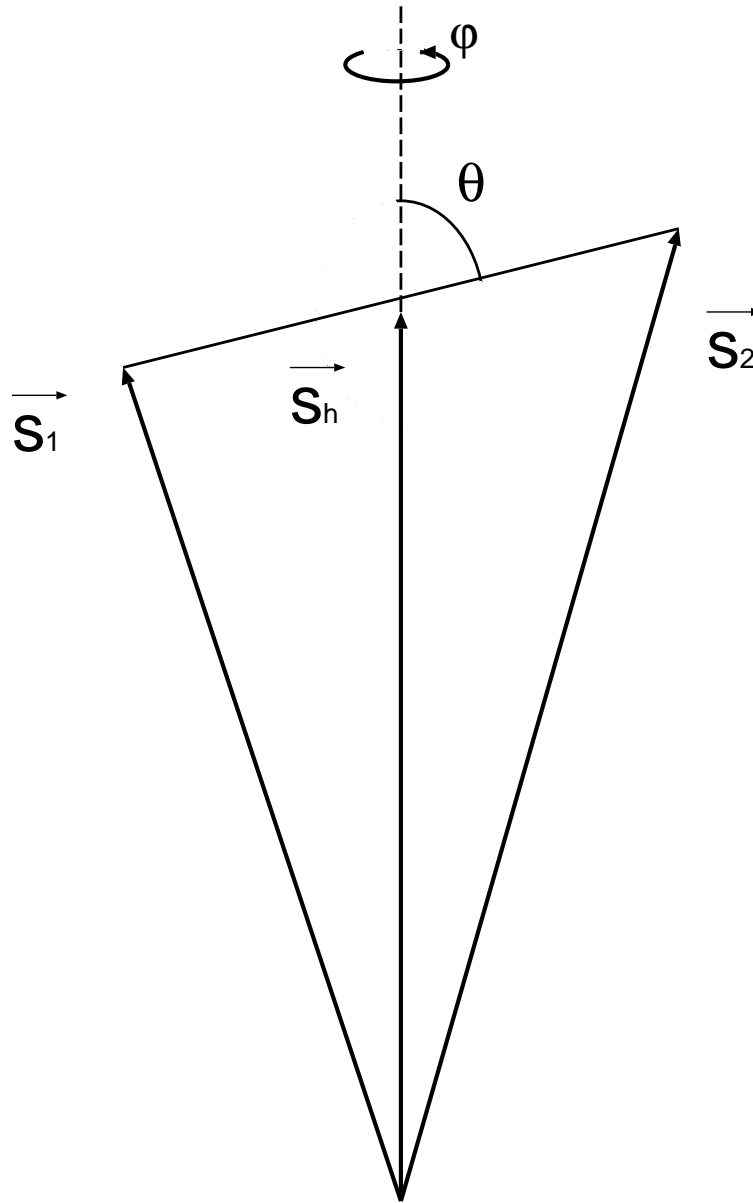


Fig. 1. A Sketch for the definition of the variables.

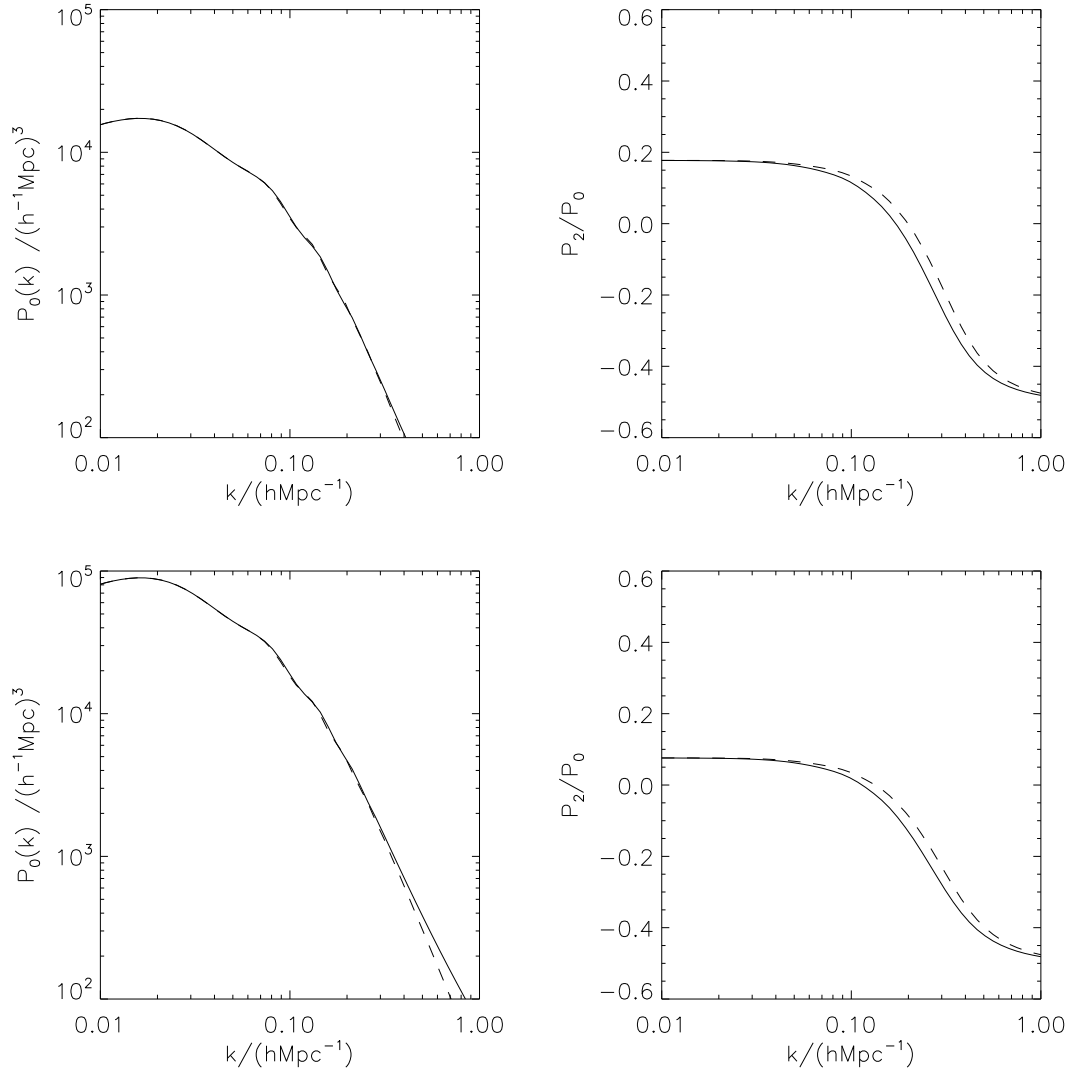


Fig. 2. Theoretical prediction for the monopole power spectrum $\mathcal{P}_0(k)$ (left panel) and quadrupole $\mathcal{P}_2(k)/\mathcal{P}_0(k)$ (right panel). The dashed curve is the linear modeling (36), while the solid curve is the nonlinear modeling (35). The upper (lower) panels assume $b_0 = 1$ ($b_0 = 2$) in the bias formula (38). Theoretical model is the Λ CDM model with the cosmological parameters $\Omega_m = 0.28$, $\Omega_b = 0.045$, $h = 0.7$, $\sigma_8 = 0.9$ and $n = 1$.

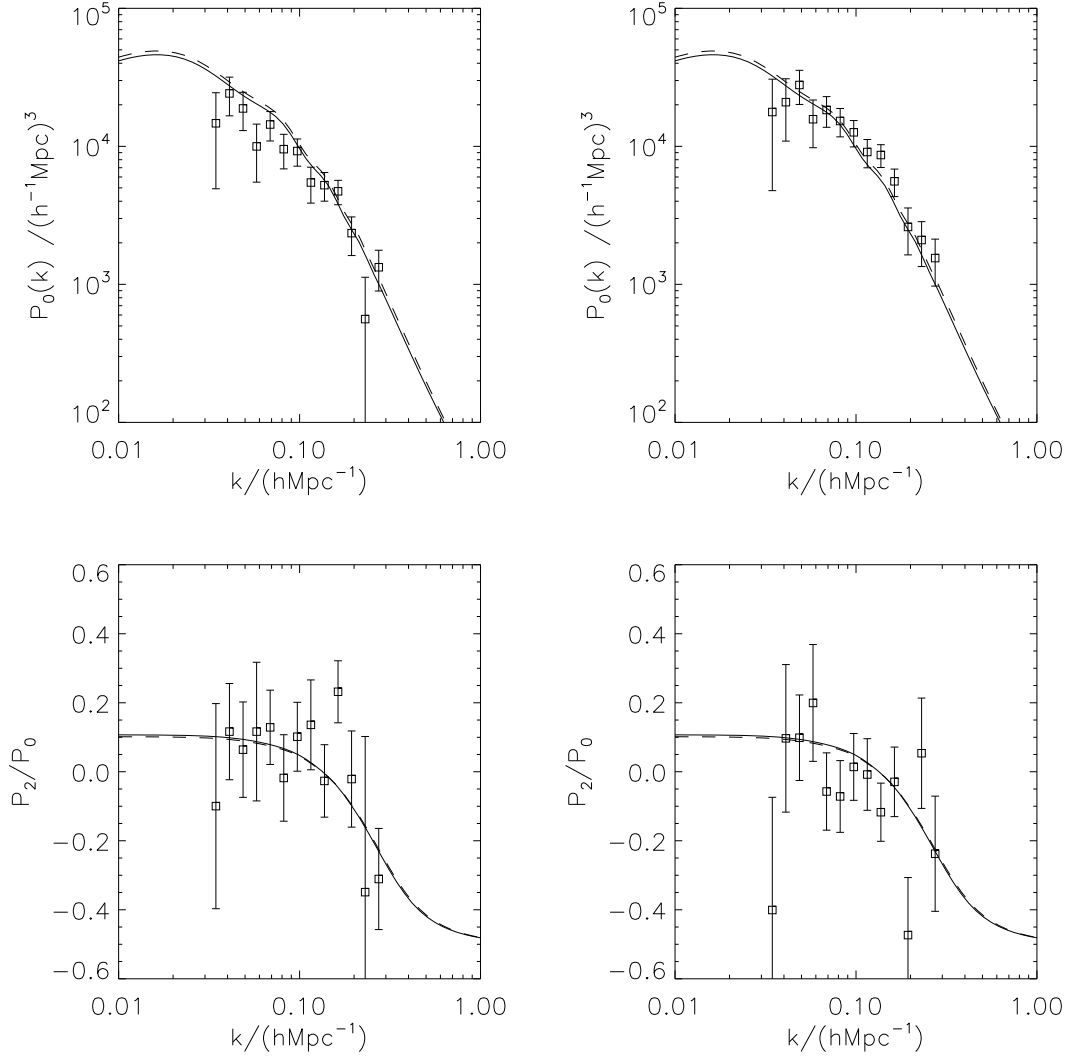


Fig. 3. The monopole power spectrum $\mathcal{P}_0(k)$ (upper panels) and quadrupole divided by monopole $\mathcal{P}_2(k)/\mathcal{P}_0(k)$ (lower panels) from the 2dF QSO sample. The left (right) panels are from the SGC (NGC) sample, respectively. The curves assume the Λ CDM model with the cosmological parameters $\Omega_m = 0.28$, $\Omega_b = 0.045$, $h = 0.7$, $\sigma_8 = 0.9$ and $n = 1$. Concerning the bias model, the solid curve assumes (38) with $b_0 = 1.5$, but the dashed curve uses (40).

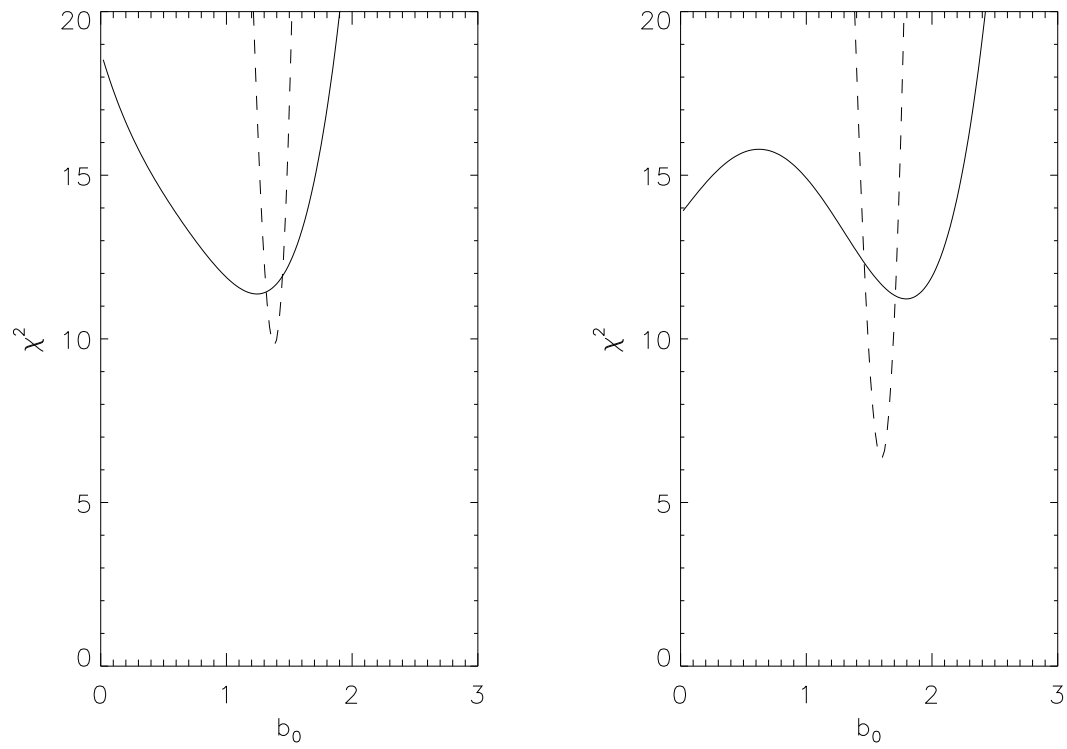


Fig. 4. The χ^2 for $\mathcal{P}_0(k)$ (dashed curve) and $\mathcal{P}_2(k)$ (solid curve) as a function of the bias parameter b_0 . The left (right) panels are for the South Galactic Cap (North Galactic Cap) sample, respectively.